01 Jan 2006

Plasma Modeling for Ultrashort Laser Ablation of Dielectrics

Lan Jiang
Missouri University of Science and Technology, jianglan@mst.edu

Hai-Lung Tsai
Missouri University of Science and Technology, tsai@mst.edu

Recommended Citation

L. Jiang and H. Tsai, "Plasma Modeling for Ultrashort Laser Ablation of Dielectrics," *Journal of Applied Physics*, American Institute of Physics (AIP), Jan 2006.
The definitive version is available at https://doi.org/10.1063/1.2216882

Plasma modeling for ultrashort pulse laser ablation of dielectrics

L. Jiang and H. L. Tsai[a)]

*Laser-Based Manufacturing Laboratory, Department of Mechanical and Aerospace Engineering,
University of Missouri-Rolla, Rolla, Missouri 65409*

In ultrashort pulse ($<$10 ps) laser ablation of dielectrics, affected materials are first transformed into absorbing plasma with metallic properties and, then, the subsequent laser-plasma interaction causes material removals. For ultrashort-pulse laser ablation of dielectrics, this study proposes a model using the Fokker-Planck equation for electron density distribution, a plasma model for the optical properties of ionized dielectrics, and quantum treatments for electron heating and relaxation time. The free electron density distribution of the plasma within the pulse duration is then used to determine the ablation crater shape. The predicted threshold fluences and ablation depths for barium aluminum borosilicate and fused silica are in agreement with published experimental data. It is found that the significantly varying optical properties in time and space are the key factors determining the ablation crater shape. The effects of fluence and pulse duration are also studied. © *2006 American Institute of Physics*. [DOI: 10.1063/1.2216882]

I. INTRODUCTION

An ultrashort pulse laser ($<$10 ps) can fully ionize almost any solid material with greatly reduced recast, microcracks, and heat-affected zone. Hence, ultrashort lasers are very promising for the microfabrication of all type of materials[1–4] especially dielectrics such as transparent materials.[3,4] Building up of free electrons is necessary in order to initialize laser ablation of dielectrics. Once the critical free electron density is created, the transparent material becomes opaque, and the absorbed energy is mainly deposited in a very thin layer within a short period of time, which leads to the ablation of the thin layer.

Energy transport within the bulk material during the ablation process can be divided into two stages:[5,6] (1) the photon energy absorption, mainly through free electrons generation, heating, and electron excitation in a time scale from a few femtoseconds to a few picoseconds and (2) the redistribution of the absorbed energy to lattice leading to material removals in a time scale from a few picoseconds to a few nanoseconds. Although many studies have been conducted, there remain many challenges in predicting ultrashort laser ablation, especially the dissipation of the absorbed energy into lattice and the corresponding material removal mechanisms.[7,8] Several material removal mechanisms such as the Coulomb explosion, electrostatic ablation, melting, and nonequilibrium thermal ablation may coexist and change from one mechanism to another during the removal process.[7] Comparing with material removals, the free electron generation and heating are much better understood.[9] Stuart *et al.* developed theories for free electron generation based on the kinetic equation and experimental results for the ablation of dielectrics at 1053, 852, and 526 nm wavelengths and 100 fs–1 ns pulsewidths.[10,11]

However, the existing models cannot be used to predict the ablation crater shape. Furthermore, the free electron heating is not properly addressed. To study free electron heating, the laser-induced electrical field inside the material must be determined which is a solution to the Maxwell equation coupling with material equation. The solution is straightforward when the optical properties of the ablation material are assumed to be constant in time and space, and independent of the incident laser intensity. With these assumptions, the free electron heating falls into the framework of the well-known skin effects. However, the optical properties of ionized material actually vary in time and space, and are laser intensity dependent under an ultrashort laser pulse.

This study proposes a plasma model by using the Fokker-Planck equation and quantum treatments to predict the ablation crater shape in dielectrics by ultrashort lasers. The comparison calculations show that for free electron generation, the contributions by electron energy diffusion, the rate of energy transfer to lattice, and the electron distribution change because of Joule heating are all negligible as compared to ionizations within the femtosecond pulse duration. As a result, the Fokker-Planck equation is simplified and the simplified equation based on the "flux-doubling" condition is also validated in this study. The model improves the accuracy of ablation depth prediction and can predict the crater shape. The effects of fluence, pulse duration, and varying optical properties are also analyzed.

II. THEORY

A. Assumptions

It is widely assumed that the ablation of dielectrics starts when the free electron density reaches the critical density.[10–13] Hence, threshold fluence can be considered as the minimal fluence that just creates the critical density.[10–13] Since the free electrons in the thin laser irradiation layer are excited up to tens of electron volts, the Coulomb explosion, electrostatic ablation, or nonequilibrium thermal ablation, instead of melting, dominate after the ionization process.[6–8,12]

---

a)Author to whom correspondence should be addressed; electronic mail: tsai@umr.edu

100, 023116-1

Thus, under an ultrashort pulse irradiation, hydrodynamic (liquid phase) motion of dielectrics is generally negligible. As a result, comparing with long pulses (>10 ps), melting and recast are greatly reduced and negligible, especially for a single ultrashort pulse ablation of dielectrics at fluences that are not much higher than the threshold fluences.[7,8] In the limit of negligible recast, ablation depth of dielectrics can be considered to be the maximum depth at which the maximum free electron density is equal to the critical density in a given processing window. Similarly, the ablation crater shape corresponds to the region at which the free electron density is greater than or equal to the critical density. These assumptions make it possible to theoretically predict threshold fluences and ablation shapes without simulating the subsequent phase change mechanisms. Our model calculates the free electron density spatial distribution as a function of time within the ultrashort pulse duration. The ablation process will certainly last for a much longer time. Because the model does not actually describe the ablation mechanisms, this study performs the calculations only until the end of the laser pulse and based on the free electron distribution, the ablation threshold, depth, and shape are predicted.

B. Free electron density distribution

This study employs the following Fokker-Planck equation to determine the free electron density distribution n_e in dielectrics under an ultrashort laser pulse,[10,11,14]

$$\frac{\partial}{\partial \varepsilon}\left[R_J n_e - \gamma E_p n_e - D \frac{\partial n_e}{\partial \varepsilon} \right] + \frac{\partial n_e}{\partial t} \equiv \frac{\partial J}{\partial \varepsilon} + \frac{\partial n_e}{\partial t} = S, \quad (1)$$

where ε is the electron kinetic energy, R_J is the heating rate of electrons, γ is the rate of electron-phonon energy transfer to the lattice, E_p is the energy of the typical phonon, D is the diffusion coefficient, J represents the direct energy change, t is the time, and S is the source or sink of electrons. The terms within the square bracket of Eq. (1) represent the electron distribution change because of Joule heating $R_J n_e$, the inelastic scattering of phonon $\gamma E_p n_e$, and electron energy diffusion $D(\partial n_e/\partial \varepsilon)$. At laser intensities greater than 10^{12} W/cm^2, the rate of energy transfer to lattice $\gamma E_p n_e$ is negligible as compared to the electron heating rate R_J within an ultrashort pulse duration.[10,11,14] The heating rate of electrons is taken as

$$R_J = \frac{\delta}{3} E^2(I), \quad (2)$$

where δ is the ac conductivity of electrons and $E(I)$ is the laser electric field, in which $I(t,r,z)$ is the laser intensity. In laser intensity $I(t,r,z)$, t is the time, r is the distance to the Gaussian beam axis, and z is the depth from the surface of the bulk material.

The ac conductivity is calculated by

$$\delta = \frac{e^2 \tau_m}{m^*[1 + \omega^2 \tau_m^2]}, \quad (3)$$

where e is the electron charge, m^* is the effective mass of an electron which is taken as the rest mass of an electron, ω is the laser frequency, and $1/\tau_m$ is the energy-dependent,

electron-phonon transport scattering rate and is estimated by[15]

$$\tau_m = \left(\frac{M}{m_e}\right)^{1/2} \frac{\hbar}{U_b} \frac{T_D}{T_l}, \quad (4)$$

where M is the atomic mass unit, m_e is the mass of electron, $\hbar = h/2\pi$ is the reduced Planck constant, U_b is the band gap energy and is 4.0 and 9.0 eV, respectively, for BBS and fused silica, T_D is the Debye temperature; and T_l is the lattice temperature in K. The diffusion coefficient is given by

$$D = 2\varepsilon R_J. \quad (5)$$

The source or sink of electrons S includes the impact ionization term S_{imp} and photoionization term (including multiphoton ionization and tunnel ionization) S_{ph} as follows:[9–11]

$$S = S_{imp} + S_{ph}. \quad (6)$$

It is assumed in impact ionization, that the two resultant electrons equally share the excess kinetic energy, and then the impact ionization term can be expressed as a function of ε and t (Ref. 10)

$$S_{imp} = 4n_e(2\varepsilon + U_b, t)\nu_I(2\varepsilon + U_b) - n_e(\varepsilon, t)\nu_I(\varepsilon), \quad (7)$$

where $\nu_I(\varepsilon)$ is the impact ionization rate described by the Keldysh's impact formula:[16]

$$\nu_I(\varepsilon) = \chi\left(\frac{\varepsilon}{U_b} - 1\right)^2$$

in which χ is a proportionality constant.

At high laser intensities ($>10^{12}$ W/cm^2), the following two assumptions can be made:[10,11,14] (1) as soon as the kinetic energy of an electron reaches the critical energy, it produces another electron, and both the electrons become zero kinetic energy and (2) the shape of electron distribution remains unchanged during the impact ionization process. The first assumption is called the flux-doubling condition. The above two assumptions can be expressed by the following conditions:[10]

$$n_e(\varepsilon \geq U_b, t) = 0, \quad J(0, t) = 2J(U_b, t). \quad (8)$$

Hence, in the limit of high laser intensities and based on the flux-doubling assumption, the impact ionization term, Eq. (7), can be simplified to the following expression:[9,10]

$$S_{imp} = a_i I(t, r, z) n_e(t, r, z), \quad (9)$$

where a_i is the impact ionization constant $a_i = 1.2 \pm 0.6$ cm^2/J for barium aluminum borosilicate (BBS) and $a_i = 4 \pm 0.6$ cm^2/J for fused silica based on experimental measurements of threshold fluence.[4]

In the case when (1) the band gap of the material is not too much greater than the photon energy, (2) there is no intermediate resonance, and (3) tunnel ionization is insignificant, the photoionization rate dominated by multiphoton ionization can be expressed as a function of laser intensity[10]

$$S_{ph} = \delta_N[I(t, r, z)]^N, \quad (10)$$

where δ_N is the cross section of N-photon ionization. $\delta_3 = 7 \times 10^{17 \pm 0.5}$ cm^{-3} ps^{-1} (cm^2/TW)^3 for BBS and $\delta_6 = 6$

$\times 10^{8\pm0.9}$ cm^{-3} ps^{-1} (cm^2/TW)^6 for fused silica at the laser wavelength around 780 nm.[4] Equation (10) does not consider the tunnel ionization. At laser intensities higher than 10^{15} W/cm^2 where tunnel ionization becomes significant, other methodologies such as the Keldysh's theory[17] should be employed to consider both multiphoton and tunnel ionizations.

Within an ultrashort pulse duration (intensities typically $>10^{12}$ W/cm^2), the lattice temperature almost remains constant and the electron heating rate is much stronger than the rate of energy transfer to lattice. Hence, the energy transfer to lattice within an ultrashort pulse duration is typically negligible in the Fokker-Planck equation. In addition, if the electron distribution change because of Joule heating and the electron energy diffusion are also neglected, Eq. (1) can be simplified to[9,10]

$$\frac{\partial n_e(t,r,z)}{\partial t} = a_i I(t,r,z) n_e(t,r,z) + \delta_N [I(t,r,z)]^N. \quad (11)$$

This study will compare the simulation results using the Fokker-Plank equation, Eq. (1), and the simplified equation, Eq. (11), to examine any differences.

C. Laser intensity and optical properties

The original laser beam before it interacts with the material is assumed to be a Gaussian distribution in time and space. It is assumed the laser focus point is at the material surface $z=0$. Considering time and space dependent optical properties, the laser intensity inside the bulk material is expressed as

$$I(t,r,z) = \frac{2F}{\sqrt{\pi/\ln 2}\, t_p}[1 - R(t,r)]$$
$$\times \exp\left[-\frac{r^2}{r_0^2} - (4\ln 2)\left(\frac{t}{t_p}\right)^2 - \int_0^z \alpha(t,r,z)dz\right], \quad (12)$$

where $R(t,r)$ is the reflectivity on the surface, $\alpha(t,r,z)$ is the absorption coefficient, r_0 is the radius of the laser beam that is defined as the distance from the center at which the intensity drops to $\exp(-1)$ of the maximum intensity, t_p is the pulse duration, and F is the laser fluence.

The optical properties of the highly ionized dielectric under an ultrashort pulse can be well determined by plasma properties.[18] This is due to the strong metallic properties of the ionized dielectrics whose free electron density under an ultrashort pulse can be increased to $10^{21}-10^{23}$ cm^{-3} that is comparable to those of metals.[10,12] Hence, the free electron model for the plasma of metals and doped semiconductors is used to determine the optical properties in the ultrashort laser dielectrics interaction. The dielectric function of plasma ϵ at a given spatial and time is expressed as[19]

$$\epsilon(t,r,z) = \epsilon_1(t,r,z) + i\epsilon_2(t,r,z) = 1 + \left[\frac{n_e(t,r,z)e^2}{m_e\epsilon_0}\right]$$
$$\times \left[\frac{-\tau_e^2(t,r,z) + i\tau_e(t,r,z)/\omega}{1 + \omega^2\tau_e^2(t,r,z)}\right], \quad (13)$$

where ϵ_0 is the electrical permittivity of free space and $\tau_e(t,r,z)$ is the free electron relaxation time. The plasma frequency ω_p is defined by[19]

$$\omega_p(n_e) = \sqrt{\frac{n_e(t,r,z)e^2}{m_e\epsilon_0}}. \quad (14)$$

For ultrashort lasers, critical density n_{cr} is selected as the free electron density at which the plasma oscillation frequency is equal to the laser frequency

$$n_{cr} = \frac{4\pi^2 c^2 m_e \epsilon_0}{\lambda^2 e^2}, \quad (15)$$

where c is the scalar speed of light in vacuum and λ is the wavelength of the laser.

The complex refractive index $\mathbf{f} = f_1 + if_2 = \sqrt{\epsilon}$ where f_1 is the normal refractive index and f_2 is the extinction coefficient, and they can be expressed as

$$f_1(t,r,z) = \sqrt{\frac{\epsilon_1(t,r,z) + \sqrt{\epsilon_1^2(t,r,z) + \epsilon_2^2(t,r,z)}}{2}}, \quad (16)$$

$$f_2(t,r,z) = \sqrt{\frac{-\epsilon_1(t,r,z) + \sqrt{\epsilon_1^2(t,r,z) + \epsilon_2^2(t,r,z)}}{2}}. \quad (17)$$

The reflectivity of the ionized material is determined by the following Fresnel expression at the surface

$$R(t,r) = \frac{[f_1(t,r,0) - 1]^2 + f_2^2(t,r,0)}{[f_1(t,r,0) + 1]^2 + f_2^2(t,r,0)}. \quad (18)$$

The absorption coefficient of laser intensity by plasma through the free electron heating $\alpha_h(t,r,z)$ is calculated by

$$\alpha_h(t,r,z) = \frac{2\omega f_2(t,r,z)}{c} = \frac{4\pi f_2(t,r,z)}{\lambda}. \quad (19)$$

However, Eq. (19) accounts for only the absorption through free electron heating but not the absorption through ionizations. The lattice temperature is assumed unchanged during the ultrashort pulse irradiation. For an ultrashort laser, the total absorption coefficient α accounting for both free electron heating absorption and ionization absorption can be determined by[10]

$$\alpha(t,r,z) = \{a_i n_e(t,r,z) + \delta_N [I(t,r,z)]^{N-1}\}[\langle\varepsilon(t,r,z)\rangle + U_b], \quad (20)$$

where $\langle\varepsilon(t,r,z)\rangle$ is the average kinetic energy of free electrons.

D. Free electron relaxation time

The free electron relaxation time in Eq. (13) must be calculated to determine the dielectric function of the plasma. In this study, the free electron relaxation time is calculated by[20]

$$\tau_e(t,r,z) = \frac{3\sqrt{m_e}[k_B T(t,r,z)]^{3/2}}{2\sqrt{2}\pi(Z^*)^2 n_e(t,r,z)e^4 \ln \Lambda}$$
$$\times \{1 + \exp[-\mu(n_e,T)/k_B T(t,r,z)]\}F_{1/2}, \quad (21)$$

where Z^* is the ionization state, k_B is the Boltzmann constant, T is the electron temperature, $F_{1/2}$ is the Fermi-Dirac integrals, μ is the chemical potential, and $\ln \Lambda$ is the Coulomb logarithm determined by $\ln \Lambda = 0.5 \ln[1 + (b_{max}/b_{min})^2]$,[21] where b_{max} is the maximum collision parameter determined by $b_{max} = (k_B T/m_e)^{1/2}/\max(\omega,\omega_p)$ and b_{min} is the minimum collision parameter determined by $b_{min} = \max[Z^* e^2/k_B T, h/2\pi(m_e k_B T)^{1/2}]$, where h is the Planck constant. For free electrons, the chemical potential can be approximated by[22]

$$\mu(n_e,T) = \varepsilon_F(n_e)\left\{1 - \frac{\pi^2}{12}\left[\frac{k_B T(t,r,z)}{\varepsilon_F(n_e)}\right]^2\right.$$
$$\left. + \frac{\pi^2}{80}\left[\frac{k_B T(t,r,z)}{\varepsilon_F(n_e)}\right]^4\right\}, \quad (22)$$

where the higher order terms are neglected and ε_F is the Fermi energy that is determined by $\varepsilon_F(n_e) = [(hc)^2/8m_e c^2] \times (3/\pi)^{2/3}[n_e(t,r,z)]^{2/3}$.

The electron temperatures are determined by the following equation:

$$c_e(T,n_e)n_e(t,r,z)\frac{\partial T(t,r,z)}{\partial t} = \alpha_h(t,r,z)I(t,r,z), \quad (23)$$

where c_e is the specific heat of free electrons $c_e(T,n_e) = (\partial\langle\varepsilon\rangle/\partial T)_V$. The average kinetic energy $\langle\varepsilon\rangle$ is calculated by the Fermi-Dirac distribution

$$\langle\varepsilon\rangle = \frac{\int_0^\infty \{1/e^{\beta(T)[\varepsilon-\mu(n_e,T)]} + 1\}\rho(\varepsilon)\varepsilon d\varepsilon}{\int_0^\infty \{1/e^{\beta(T)[\varepsilon-\mu(n_e,T)]} + 1\}\rho(\varepsilon)d\varepsilon}, \quad (24)$$

where $\beta(T) = 1/k_B T(t,r,z)$ and $\rho(\varepsilon)$ is the density of states expressed by

$$\rho(\varepsilon) = \frac{8\sqrt{2}\pi m_e^{3/2}}{h^3}\sqrt{\varepsilon}. \quad (25)$$

Our model predicts the free electron density distribution within the pulse duration using the Fokker-Planck equation, for which, the laser intensity distribution, optical properties, electron temperatures, and other parameters are calculated numerically as functions of time and space. The threshold fluence is determined when the free electron density at the material surface is equal to the critical density at the end of laser irradiation for a given laser wavelength and pulse duration. A small volume of material is ablated if its free electron density becomes greater than or equal to the critical density.

III. RESULTS AND DISCUSSION

A. Fixed processing window

The example of the ablation of BBS using a 780 nm, 220 fs laser is calculated and compared with experimental results. The experimental ablation threshold fluence is 3.2 ± 0.6 J/cm^2 and the corresponding experimental ablation depth at 6.2 ± 0.7 J/cm^2 is 270 ± 65 nm.[4] Our model using Eqs. (1) and (11) give the same predictions: 3.3 J/cm^2 for the threshold fluence and 260 nm for the ablation depth at 6.2 J/cm^2, which demonstrates that for free electron generations, the electron energy diffusion and electron distribution change because of Joule heating are negligible within the femtosecond pulse duration t_p. This conclusion is confirmed by Fig. 1(a) that shows the distribution of free electron density predicted by Eq. (1) is visually overlapped with that by Eq. (11). More precisely, our comparison calculations show that for free electron generation in this case, the contribution of electron energy diffusion and that of the electron distribution change because of Joule heating are two and four orders of magnitudes, respectively, smaller than the contributions of ionizations within the pulse duration t_p. Also, since the electron heating rate is much stronger than the rate of energy transfer to lattice within t_p,[7,8] the results also indirectly confirm that the rate of energy transfer to lattice is negligible within t_p. Hence, the use of Eq. (11) simplified from the Fokker-Planck equation is well justified. Figure 1(a) also shows that in the first 25 fs, at $r=0$ in the surface layer, photoionization (multiphoton ionization) dominates the initial ionization process until the free electron density reaches 4.6×10^{19} cm^{-3}. On the other hand, the overall contribution of impact ionization 2.17×10^{21} cm^{-3} is about one order of magnitude greater than that of photoionization 4.84×10^{20} cm^{-3}. The critical density is created at about 95 fs. Within t_p, the reflectivity at $r=0$ in the surface layer is quite low at the initial stage of the pulse irradiation as shown in Fig. 1(b). From 80 to 110 fs, the reflectivity increases rapidly from a low level to about 0.87. Hence, the laser energy after the formation of critical density is mainly reflected. Note the reflectivity in our calculations is always greater than zero as indicated in Eqs. (13)–(18). For example, the theoretical reflectivity is 1.4×10^{-3} at 50 fs. However, because the reflectivity values (on the order of 10^{-3} or less) are so small for times less than 60 fs, the reflectivity read like zero in Fig. 1(b). After the free electron density becomes comparable to the critical density, the Gaussian beam is strongly shaped by the plasma, as shown in Fig. 1(c).

As for the distributions in the space domain, optical property changes with radius are demonstrated in Fig. 2. The overall reflectivity integrated in the whole time domain significantly decreases with the radius r. At $r=0$ where the peak free electron density occurs, the overall reflectivity is the highest, 0.549, while it drops to 0.023 at $r=40$ μm. The reflectivity distribution shapes the Gaussian beam profile to become more flat. Another important optical property for crater shape is the absorption coefficient. A sample absorption coefficient distribution at $t=110$ fs in the surface layer is also plotted in Fig. 2, which illustrates a strong negative correlation between the radius and absorption coefficient.
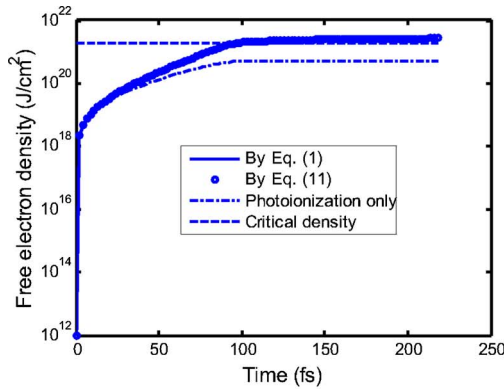
(a)
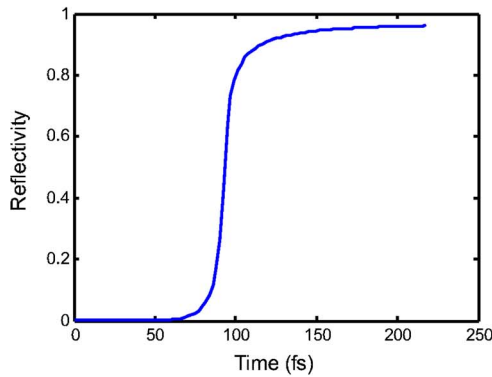
(b)
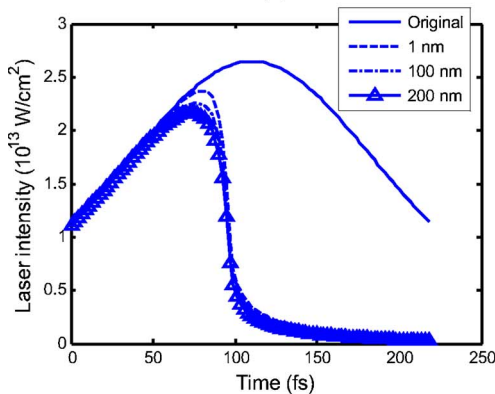
(c)

FIG. 1. Time-dependent properties of BBS at $r=0$, $F=6.2$ J/cm^2 by a 780 nm, 220 fs laser. (a) Free electron density in the surface layer (numerically 1 nm), (b) surface reflectivity, and (c) transmitted laser intensity.

Due to the changes of optical properties in time and space, the laser beam transmitted into the plasma layers is strongly shaped.

The ablation depth is determined by free electron density along the material depth direction at $r=0$ and $t=220$ fs, as shown in Fig. 3. The layer at 260 nm is identified as the ablation depth, at which the free electron density just reaches the critical density.

B. The effects of fluence

The shape of the ablation crater strongly depends on the laser fluence. Figure 4 presents the effects of fluences for a 780 nm, 220 fs laser ablation of BBS. At a higher fluence, a greater percentage of the absorbed laser energy is deposited
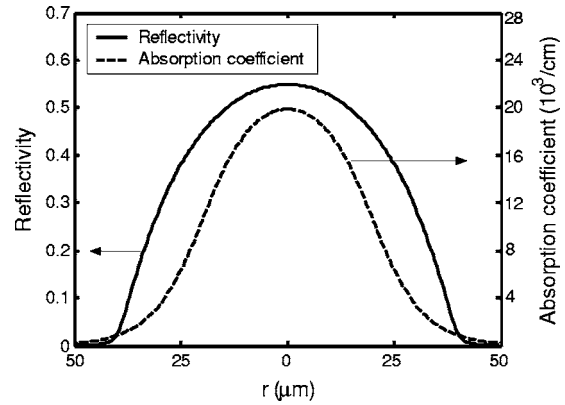

FIG. 2. Radius-dependent optical properties of BBS in the ionized dielectrics at $F=6.2$ J/cm^2 by a 780 nm, 220 fs laser: overall reflectivity integrated in time domain and absorption coefficient at $t=110$ fs in the surface layer (numerically 1 nm).

in a thin layer, as shown in Fig. 4(a). At 2 J/cm^2 that is lower than the threshold fluence, only 0.79% of the absorbed energy is deposited in the first 500 nm. The percentages for the same depth (500 nm) at 6.2 and 20 J/cm^2 are 14.3% and 28.9%, respectively, which are quite striking. The formation of a thin skin depth at fluences higher than the threshold fluence is very obvious, which strongly affects the ablation crater shape. The ablation shapes by a 780 nm, 220 fs laser at three different fluences are shown in Fig. 4(b). The bottom of the crater at 6.2 J/cm^2 is rather flat as compared to the original Gaussian beam profile. The flat bottom crater at 10 J/cm^2 is even more obvious. Such type of flat-bottom crater shapes have been observed in previous experiments on ultrashort laser ablation of other materials.[1,23–25] A flat-bottom crater occurs because of the overall reflectivity and absorption coefficient significantly increase with the increase of fluence as shown in Fig. 4(c). For $r=0$ and $t=110$ fs, the absorption coefficients in the surface layer (numerically 1 nm) at 3.8, 6.2, and 10 J/cm^2 are 0.18×10^4, 2.0×10^4, and 4.2×10^4 cm^{-1}, respectively. The overall reflectivity integrated in the whole pulse duration at the fluences of 3.8, 6.2, and 10 J/cm^2 are 0.16, 0.55, and 0.76, respectively. Accordingly, as shown in Fig. 4(d), the changes of ablation depths by the 780 nm, 220 fs laser as a function of the fluence well explain the crater shapes plotted in Fig. 4(b).
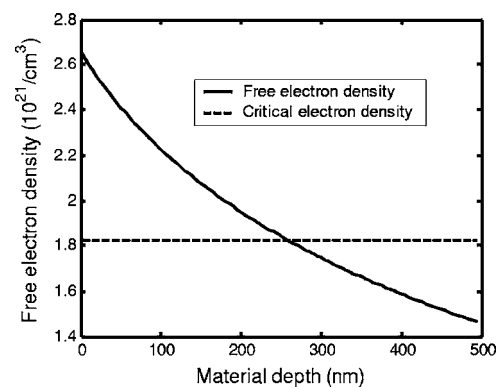

FIG. 3. Depth-dependent free electron density of BBS at $t=220$ fs, $r=0$, $F=6.2$ J/cm^2 by a 780 nm, 220 fs laser.
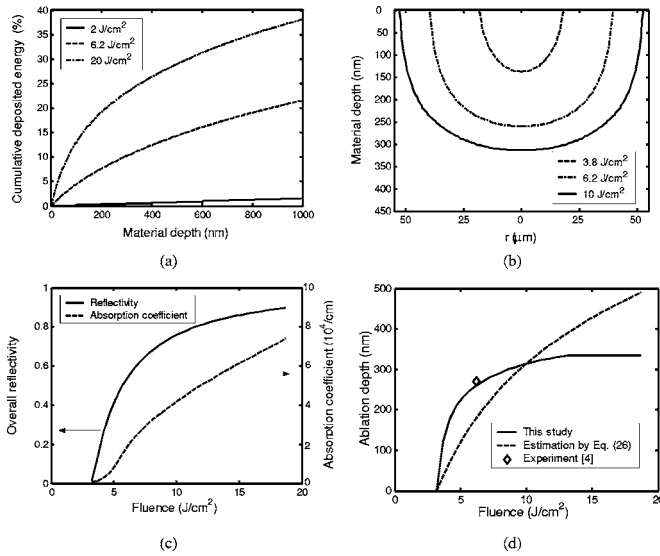
FIG. 4. The effects of fluence for a 780 nm, 220 fs laser ablation of BBS: (a) cumulative percentages of laser energy deposited in different depths, (b) ablation crater shapes, (c) overall reflectivity and absorption coefficient in the surface layer (numerically 1 nm) at $t = 110$ fs, and (d) ablation depths.

Based on the Beer's law with constant optical properties, the following equation has been used to predict the ablation depth as a function of fluence:[26]

$$d = \left(\frac{1}{\alpha}\right)\ln \frac{F}{F_{\text{th}}}, \tag{26}$$

where F_{th} is the threshold fluence. As the absorption coefficient of the material varies significantly as a function of time, space, and laser intensity during the femtosecond laser irradiation, the selection of a "correct" constant absorption coefficient is very challenging if not impossible. If a mean absorption coefficient over the space and the fluence is used, Eq. (26) predicts the ablation depth as shown in Fig. 4(d), which is not consistent with the experimental result. As shown in Fig. 4(d), our predicted ablation depth by the 780 nm, 220 fs laser increases from 0 to 210 nm in the fluence range of 3.26–4.7 J/cm^2 that is 1–1.44 times of the theoretical threshold fluence. In this fluence range, because a possible fluctuation of the fluence will lead to a high variation of ablation depth, it is technically very difficult to control the ablation depth precision of BBS below 210 nm using the 780 nm, 220 fs laser. This explains the poor repeatability and controllability in ultrashort laser nanomachining using fluences slightly above the threshold fluence. On the other hand, from about 5.0 to 18.7 J/cm^2, the ablation depth increases relatively slow. The existence of a nearly constant ablation depth after a steep increase was experimentally observed before.[27–29] Note the constant ablation depth exists only in a limited fluence range and the ablation depth may significantly increase if the fluence continues to increase.[28,29]

C. The effects of pulse duration

As shown in Fig. 5(a), at fixed wavelength (780 nm) and fluence (6.2 J/cm^2) and at the peak intensities ($t_p/2$), the absorption coefficient and the overall reflectivity decrease with the increase of the pulse duration for BBS. On the other
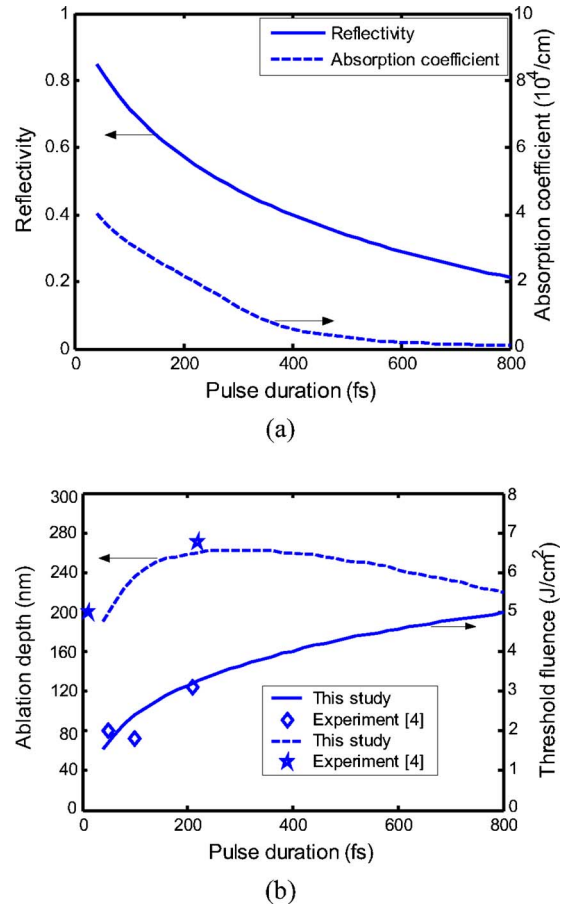

FIG. 5. The effects of pulse duration for a 780 nm, 220 fs laser ablation of BBS at 6.2 J/cm^2: (a) overall reflectivity and absorption coefficient in the surface layer (numerically 1 nm) at peak intensities and (b) threshold fluence and ablation depth.

hand, Fig. 5(b) shows that the threshold fluence increases with the pulse duration as expected. Our predicted threshold fluences of BBS at different pulse durations are in agreement with experimental data.[4] However, the ablation depth by a 780 nm laser at 6.2 J/cm^2 is not a monotonous function of the pulse duration. When the pulse duration is very short and the laser fluence is "strong" with respect to the corresponding threshold fluence, the ablation depth increases as the pulse duration increases. Figure 5(b) shows that the ablation depth increases with the increase of pulse duration in the range of 40–240 fs. However, when the pulse duration increases to some point, the fluence becomes "weak" with respect to the corresponding threshold fluence, thereafter the ablation depth decreases as the pulse duration increases. Figure 5(b) shows that ablation depth decreases with the increase of pulse duration in the range of 360–800 fs.

D. Fused silica

The example of a 780 nm, 50 fs laser ablation of fused silica is also calculated to confirm the conclusions from BBS. The band gap of fused silica is 9.0 eV. The impact ionization coefficient, $a_i = 4 \pm 0.6$ cm^2/J, and the cross section of N-photon absorption, $\delta_6 = 6 \times 10^{8\pm0.9}$ cm^{-3} $ps^{-1}(cm^2/TW)^6$ at the laser wavelength of 780 nm.[4] The experimental ablation threshold fluence is about 3.3 J/cm^2, and the corre-
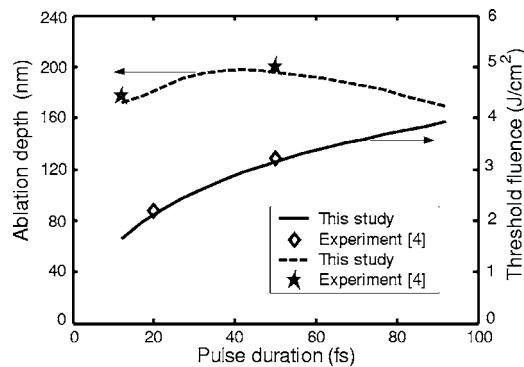
FIG. 6. The effects of pulse duration for a 780 nm, 50 fs laser ablation of fused silica: threshold fluence and ablation depth at 5 J/cm^2.

sponding experimental ablation depth at 5 J/cm^2 is about 200 nm.[4] The proposed model gives the results of 3.15 J/cm^2 and 195 nm, respectively, for the threshold fluence and ablation depth at 5 J/cm^2. As shown in Fig. 6, the patterns of threshold fluence and ablation depth at 5 J/cm^2 for fused silica as a function of the pulse duration are similar to those in Fig. 5 for BBS.

IV. CONCLUSIONS

This study proposes a plasma model for ultrashort laser ablation of dielectrics. The Fokker-Planck equation is employed to investigate the free electron generation and distribution. The free electron model for plasma of metals and doped semiconductors is modified to study time, space, and laser intensity dependent optical properties of ionized material under the ultrashort laser-plasma interaction. The ablation threshold fluences and depths predicted by the proposed model are in good agreement with experimental measurements in the examples of BBS and fused silica. The comparison calculations show that for free electron generation, the contributions by electron energy diffusion, the rate of energy transfer to lattice, and the electron distribution change because of Joule heating are negligible as compared to ionizations within the femtosecond pulse duration. It is found that the significantly varying optical properties of the laser-induced plasma can greatly affect the laser beam profile in the material and, as a result, the ablated crater shape. The proposed model improves the accuracy of ablation depth prediction and can predict the crater shape in ultrashort laser ablation of dielectrics.

[1]G. Dumitru, V. Romano, H. P. Weber, M. Sentis, and W. Marine, Appl. Phys. A: Mater. Sci. Process. **74**, 729 (2001).
[2]L. Jiang and H. L. Tsai, ASME J. Heat Transfer **127**, 1167 (2005).
[3]P. P. Pronko, S. K. Dutta, D. Du, and R. K. Singh, J. Appl. Phys. **78**, 6233 (1995).
[4]M. Lenzner, J. Krüger, S. Sartania, Z. Cheng, C. Spielmann, G. Mourou, W. Kautek, and F. Krausz, Phys. Rev. Lett. **80**, 4076 (1998).
[5]X. Liu, D. Du, and G. Mourou, IEEE J. Quantum Electron. **33**, 1706 (1997).
[6]F. Ladieu, P. Martin, and S. Guizard, Appl. Phys. Lett. **81**, 957 (2002).
[7]L. Jiang and H. L. Tsai, *Proceedings of NSF Workshop on Research Needs in Thermal, Aspects of Material Removal*, Stillwater, OK, 2003, p. 163
[8]R. Stoian, D. Ashkenasi, A. Rosenfeld, and E. E. B. Campbell, Phys. Rev. B **62**, 13167 (2000).
[9]A. Tien, S. Backus, H. Kapteyn, M. Murnane, and G. Mourou, Phys. Rev. Lett. **82**, 3883 (1999).
[10]B. C. Stuart, M. D. Feit, S. Herman, A. M. Rubenchik, B. W. Shore, and M. D. Perry, Phys. Rev. B **53**, 1749 (1996).
[11]B. C. Stuart, M. D. Feit, A. M. Rubenchik, B. W. Shore, and M. D. Perry, Phys. Rev. Lett. **74**, 2248 (1995).
[12]E. G. Gamaly, A. V. Rode, B. Luther-Davies, and V. T. Tikhonchuk, Phys. Plasmas **9**, 949 (2002).
[13]D. Du, X. Liu, G. Korn, J. Squier, and G. Mourou, Appl. Phys. Lett. **64**, 3071 (1994).
[14]M. D. Perry, B. C. Stuart, P. S. Banks, M. D. Feit, V. Yanovsky, and A. M. Rubenchik, J. Appl. Phys. **85**, 6803 (1999).
[15]E. M. Lifshitz and L. P. Pitaevskii, *Physical Kinetics* (Pergamon, Oxford, 1981).
[16]B. K. Ridley, *Quantum Processes in Semiconductors* (Clarendon, Oxford, 1993).
[17]L. V. Keldysh, Sov. Phys. JETP **20**, 1307 (1965).
[18]B. Rethfeld, A. Kaiser, M. Vicanek, and G. Simon, Phys. Rev. B **65**, 214303 (2002).
[19]M. Fox, *Optical Properties of Solids* (Oxford University Press, Oxford, 2001).
[20]Y. T. Lee and R. M. More, Phys. Fluids **27**, 1273 (1984).
[21]K. Eidmann, J. Meyer-ter-Vehn, T. Schlegel, and S. Hüller, Phys. Rev. E **62**, 1202 (2000).
[22]N. W. Ashcroft and N. D. Mermin, *Solid State Physics* (Holt, Rinehart, and Winston, New York, 1976).
[23]A. S. Zakharov, M. V. Volkov, I. P. Gurov, V. V. Temnov, K. Sokolovski-Tinten, and D. von der Linde, J. Opt. Technol. **69**, 478 (2002).
[24]Z. Wu, H. Jiang, Z. Zhang, Q. Sun, H. Yang, and Q. Gong, Opt. Express **10**, 1244 (2002).
[25]J. Bonse, M. Munz, and H. Sturm, IEEE Trans. Nanotechnol. **3**, 358 (2004).
[26]J. Krüger and W. Kautek, Laser Phys. **9**, 30 (1999).
[27]S. Kurosaki, M. Kuriyama, and Y. Ito, *Machining of Micro-Holes on a Thin Glass Plate by Femtosecond Laser Pulses*, Proceeding of ICALEO, Jacksonville, FL (2001).
[28]M. Lapczyna, K. P. Chen, P. R. Herman, H. W. Tan, and R. S. Marjoribanks, Appl. Phys. A: Mater. Sci. Process. **69**, S883 (1999).
[29]P. R. Herman, A. Oettl, K. P. Chen, and R. S. Marjoribanks, Proc. SPIE **3616**, 148 (1999).